CARBON XXX (2008) XXX–XXX

available at www.sciencedirect.com

ScienceDirect

journal homepage: www.elsevier.com/locate/carbon

Effect of surface chemistry on electrochemical storage of hydrogen in porous carbon materials

M.J. Bleda-Martínez[a], J.M. Pérez[b], A. Linares-Solano[a], E. Morallón[b], D. Cazorla-Amorós[a,*]

[a]Departamento de Química Inorgánica, Universidad de Alicante, Ap. 99, E-03080 Alicante, Spain
[b]Departamento de Química-Física, Universidad de Alicante, Ap. 99, E-03080 Alicante, Spain

ARTICLE INFO

Article history:
Received 24 May 2007
Accepted 19 March 2008

ABSTRACT

Porous carbon materials, with different porosities and surface chemistry have been prepared and characterized to obtain a better understanding of the mechanism of the electrochemical storage of hydrogen. The hydrogen storage capacity depends, not only on the porosity of the material, but also on the surface chemistry, which is a critical factor. The results show that the higher the amount of surface oxygen groups, the lower is the hydrogen uptake. Measurement of the number of active carbon sites shows the important role of the unsaturated carbon atoms in the process. In situ Raman spectroscopy has been used in order to further explore the structural changes in the carbon material during the charge–discharge processes. This technique has allowed us to observe the formation of the C(sp^2)—H bonds during the cathodic process and its reversibility during the oxidation step.

1. Introduction

Carbon materials have been extensively studied as electrodes for energy storage devices since they present a very interesting electrochemical behaviour. These materials may have high electrical conductivity and can both donate and accept electrons [1]. Carbon electrodes have a good polarizability and their properties are tuneable depending on the porosity, thermal treatment, microtexture, hybridization, content of heteroatoms, etc. Moreover, they are chemically stable in most solvents and present relatively low cost and easy processability [2]. One important application is in rechargeable batteries in which carbon materials are used as a lithium reservoir at the negative electrode [1]. Additionally, the storage of energy in supercapacitors, based on the electrical double layer and pseudocapacitance of carbon materials, has also been deeply analysed with very promising results [2–4].

A different electrochemical application is the electrochemical storage of hydrogen by electrodecomposition of water in alkaline medium at cathodic conditions. Several nanostructured carbon materials, mainly nanotubes (CNT), have been tested for this application [5–11]. However, the results obtained present an important scattering. In fact, taking into account theoretical calculations and experimental results, it is highly unlikely that a significant amount of hydrogen can be stored in CNT [8]. The different results could be justified by the different degree of purity of the samples (CNT often contain amorphous and disordered carbonaceous material or residual metal catalyst) [8,12].

Porous carbons have also been extensively studied for this application, giving higher values for hydrogen storage and much better reproducibility. Probably, the most relevant research in this area has been done by Beguin, Frackowiak and co-workers [13–19]. Similar results have been obtained by other authors using ordered porous carbons with tailored pore size [12], carbon blacks [20] or necklace-like hollow carbon nanospheres [21]. From these studies, the role of porosity has been discussed as well as the importance of the dangling carbon atoms in the hydrogen storage. In general, the higher the narrow porosity, the higher the hydrogen uptake [16] and

* *Corresponding author:* Fax: +34 965 903537.
E-mail address: cazorla@ua.es (D. Cazorla-Amorós).
0008-6223/$ - see front matter © 2008 Published by Elsevier Ltd.
doi:10.1016/j.carbon.2008.03.016

the uptake decreases with decreasing the number of dangling atoms [15].

However, the role of surface chemistry has not been discussed in detail in the previous work done on this topic and the experimental evidence of the mechanism of hydrogen storage remains unknown. Thus, in this work, we have analysed the effect of the surface oxygen complexes on the electrochemical storage of hydrogen; additionally, in situ Raman spectroscopy has been used to get information on the structural changes occurring in the carbon material during the charge–discharge process and the type of interaction between hydrogen and carbon.

2. Experimental

2.1. Activation process

Chemical activation was done in N_2 (800 ml/min) at 750 °C (1 h at this maximum temperature), using KOH as activating agent and an anthracite as precursor. Details of the preparation process are available elsewhere [22]. The activating agent to carbon ratio for each sample are included in Table 1.

2.2. Chemical oxidation with HNO_3

Sample Cp was subjected to chemical oxidation with HNO_3 in order to produce a large amount of surface oxygen complexes. The oxidation was carried out by mixing 1.5 g of activated carbon (Cp) with 20 ml of concentrated nitric acid during 3 h at room temperature. After this treatment, the sample was washed several times with hot distilled water until the pH of the filtrate was the same as the washing water. Then, the sample was dried at 100 °C.

Table 1 – Activating agent/carbon ratio in chemical activation

Sample	Activating agent/carbon ratio
Ap	1:1
Bp	2:1
Cp	3:1

2.3. Thermal treatments in N_2

Activated carbons with different amounts of surface oxygen complexes were obtained by subjecting the oxidized sample Cp to thermal treatments at different temperatures (from 300 to 900 °C). These treatments were carried out in N_2 (200 ml/min) and using a heating rate of 5 °C/min. After reaching the heat-treatment temperature, it was kept for 1 h. Temperatures used are shown in Table 2. Additionally, samples Ap and Bp were heat treated at the same conditions up to 900 °C in order to remove most of the oxygen complexes. With this series of samples, we can compare the behaviour of materials with different porosity and similar surface chemistry (i.e., samples C6, B and A) and materials with similar porosity and different surface chemistry (i.e., samples C1–C6) (Table 2).

2.4. Porous texture characterization

Porous texture of all samples was determined by physical adsorption (N_2 at 77 K and CO_2 at 273 K) using an automatic adsorption system (Autosorb-6, Quantrachrome) after samples out-gassing at 523 K under vacuum for 4 h. The total micropore volume was calculated from the application of the Dubinin–Radushkevich equation to the N_2 adsorption at 77 K. The narrow micropore volume (i.e., pore size smaller than around 0.7 nm) has been assessed from CO_2 adsorption at 273 K using the DR equation and for relative pressures below 0.025. The densities of the adsorbed phases used for the calculations, were 0.808 and 1.023 g/ml for N_2 and CO_2, respectively [23].

2.5. Active surface area characterization

The active surface area (ASA) gives a measurement of the number of reactive carbon atoms or active carbon sites of a carbon sample. The ASA of samples C6, B and A was estimated by a modification of the Laine et al. method [24]. Firstly, the samples were treated up to 950 °C in helium to remove the surface complexes present as a result of the previous activation process. The ASA was then determined from the amount of surface oxygen complexes formed at 300 °C in synthetic air flow during 7 h (a longer time did not result in an increase the weight of the sample). The number of oxygen complexes can be determined either from the weight uptake of the samples

Table 2 – Thermal treatment temperature, porous texture, surface chemistry characterization, % wt of hydrogen electrochemically storage and active surface area (ASA) for the different samples

Pristine sample	Sample	T (thermal treatment) (°C)	BET surface area (m^2/g)	V_{DR} (N_2) (cm^3/g)	V_{DR} (CO_2) (cm^3/g)	μmol CO/g	μmol CO_2 /g	% wt H	ASA (m^2/g)
Cp	C1	–	2340	1.14	0.64	5026	2610	0.58	–
Cp	C2	300	2380	1.16	0.62	4066	2063	0.71	–
Cp	C3	450	2450	1.18	0.62	4520	1134	0.82	–
Cp	C4	600	2435	1.17	0.62	2662	747	0.86	–
Cp	C5	750	2250	1.14	0.59	747	313	0.94	–
Cp	C6	900	2270	1.07	0.58	229	260	0.94	27
Bp	B	900	1655	0.81	0.54	240	271	0.73	19
Ap	A	900	930	0.45	0.43	208	212	0.42	17

or measuring the CO and CO_2 desorbing groups in a subsequent temperature programmed desorption (TPD) experiment [25]. We chose the former method. We have used a TA thermobalance (SDT 2960) with a sensitivity of 1 μg; the error of the ASA, obtained from the measurement of at least three samples of the same material, is within 5%.

2.6. Surface chemistry characterization

Temperature programmed desorption experiments were done in a DSC-TGA equipment (TA Instruments, SDT 2960 Simultaneous) coupled to a mass spectrometer (Thermostar, Balzers, GSD 300 T3), to characterize the surface chemistry of all samples. In these experiments, 5 mg of the sample were heated up to 950 °C (heating rate 20 °C/min) under a helium flow rate of 100 ml/min.

2.7. Electrochemical characterization

For the electrochemical characterization, composite electrodes were prepared from powder porous carbon material, acetylene black (Strem Chemicals) and binder (PTFE, aqueous dispersion (60% solids), Aldrich), in a ratio 80:10:10 wt%, respectively. The materials were mixed and deposited over a graphite current collector. The total electrode weight used for the measurements was about 20 mg. The standard three electrode cell configuration was employed. Reversible hydrogen electrode (RHE) was used as reference and a platinum wire was employed as a counter electrode; however, all the potentials have been referred to the normal hydrogen electrode (NHE). 6 M KOH was used as aqueous electrolyte.

In this work, the term *charge* refers to the negative polarization of the electrode. The term *discharge* is used for the positive polarization. The galvanostatic charging process was carried out with a high current density (−500 mA/g). The reasons for this excess of charge are explained in [18]. The hydrogen uptake was evaluated from the charge consumed in the oxidation step (at 25 mA/g), subtracting the corresponding double layer charge, determined previously by cyclic voltammetry at 5 mV/s.

All electrochemical measurements were carried out with an EG&G Potentionstat/Galvanostat model 273 controlled by software ECHEM M270. All the solutions were prepared with ultrapure water (Purelab ELGA).

2.8. In situ RAMAN spectroscopy characterization

The Raman spectra were obtained with a LabRam spectrometer (Jobin–Yvon Horiba). The excitation line was provided by a 17 mW He–Ne laser at 632.8 nm for sample C6; a given spectrum corresponds to the average of four measurements with an acquisition time of 40 s for each of them. The calibration of the spectrometer was performed with a slice of Si (521 ± 2 cm^{-1}). The laser beam was focused through a 50 × long-working objective (0.5 NA) into a 2 μm spot at the electrode surface. The sample viewing system consisted of a television camera attached to the microscope. The spectrometer resolution was better than 3 cm^{-1} and the detector was a Peltier cooled charge-couple device (CCD) (1064 × 256 pixels). The slit and confocal pinhole were set to 200 and 600 mm and a 600 lines grating was employed. The excitation line used in the case of sample C1 was a 784.8 nm diode laser because with the excitation line of 632.8 nm the fluorescence hides any spectrum as a consequence of the high oxygen content in this sample; in this case, the acquisition time was 60 s and 4 averages were performed. All the spectra are presented as obtained.

The carbon samples were deposited on a glassy carbon disc (3 mm in diameter) sheathed in a PTFE piece. This substrate is then mounted on a spectroelectrochemical PTFE cell designed to acquire in situ Raman spectra. The cell was designed with a silica window to form a closed system in order to prevent the etching of the lens. More details on the spectroelectrochemical cell can be found in reference [26]. A Pt wire was used as a counterelectrode, whereas a saturated Ag/AgCl electrode was used as reference electrode contacting the working solution (6 M KOH) through a Luggin capillary. The potentials are referred as the normal hydrogen electrode.

3. Results and discussion

3.1. Porous texture and surface chemistry by TPD

The activated carbons prepared present type I isotherms, what is characteristic of microporous solids. Table 2 contains the BET surface area and the micropore volumes calculated from N_2 adsorption data at 77 K [$V_{DR}(N_2)$] and CO_2 adsorption data at 273 K [$V_{DR}(CO_2)$] for each sample.

It can be observed that samples from C1 to C6 have very similar porosities, being the fraction of narrow microporosity ($V_{DR}(CO_2)/V_{DR}(N_2)$) close to 54% in all these samples. Samples C6, B and A have different BET surface areas and also different pore size distributions, being sample A the one presenting the highest fraction of narrow microporosity.

When the carbon materials are subjected to TPD experiments, surface oxygen groups decompose producing CO and CO_2 at different temperatures. The quantification of the amount of these compounds desorbed in the TPD experiments is included in Table 2. It can be observed that samples from C1 to C6 present a very different surface chemistry, while samples A, B and C6 have a similar content in surface oxygen groups.

3.2. Electrochemical characterization

Figs. 1 and 2 present the results obtained from the galvanostatic charge–discharge for all the materials. In the first one, the results for samples C6, B and A, are shown. The shape of the curves is similar in the three samples. During the discharge process until the same final potential, a plateau at about −0.7 V is observed, indicating the oxidation of the hydrogen trapped in the carbon sample. This plateau is clearer in samples B and C6. Sample C6, with the highest porosity presents a better performance for this application, since the charge delivered is higher. The slope of the final part of the curves, from −0.47 to −0.27 V, depends on the surface area of the material, since it is mainly related to the double layer contribution. The higher the slope, the lower the capacitance, in agreement with the lower porosity of the material. Fig. 2 shows the same plots for samples from C1 to C6. Although the porosity of the samples is very similar, the elec-

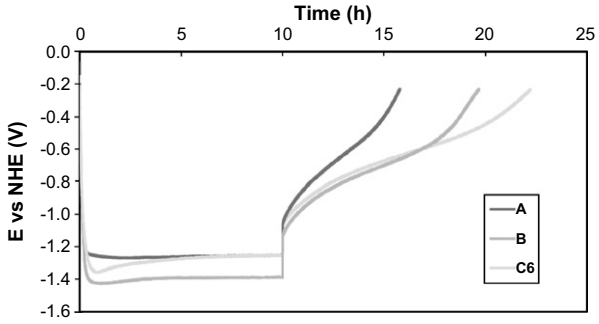

Fig. 1 – Galvanostatic charge/discharge curves for samples C6, B and A. 6 M KOH.

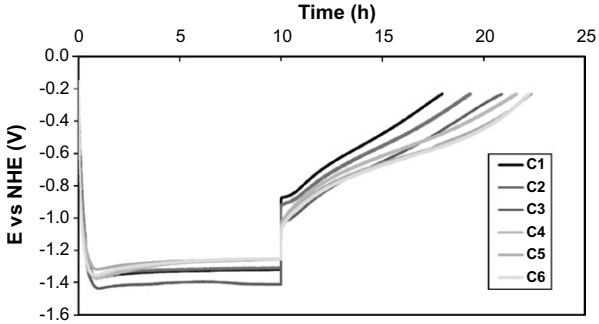

Fig. 2 – Galvanostatic charge/discharge curves for samples from C1 to C6, 6 M KOH.

trochemical behaviour is different. Sample C1, the one with the highest amount of surface oxygen complexes hardly presents a defined oxidation plateau. As the oxygen content decreases, the oxidation plateau appears more clearly.

Fig. 3 plots the hydrogen electrochemically stored vs. the $V_{DR}(N_2)$ for all the samples studied, taking into account the oxidation charge, once subtracted the double layer contribution.

It can be observed that when the amount of surface oxygen complexes is low, the hydrogen storage keeps a linear relationship with the porosity of the material. A very similar relationship is found if the wt% of hydrogen stored is plotted against the $V_{DR}(CO_2)$ (not shown). Other researchers have published a linear trend followed by the porosity and the percentage of hydrogen electrochemically stored [19,20]. Nevertheless, they have also found deviations from this trend [16], and have explained them with the pore size distribution. Thus, it seems that the narrow porosity between 0.6 and 0.7 nm is the responsible for the hydrogen storage [16] and that the wider porosity does not improve the performance of the porous carbon material as a hydrogen reservoir. However, this approximation is not completely satisfactory, since the correlation between the narrow porosity (0.6–0.7 nm) and the hydrogen stored does not cross the origin [16].

However, if the porosity is kept almost constant but the surface chemistry is modified by increasing the amount of surface oxygen groups, the hydrogen storage decreases dramatically (Fig. 3). This can be observed more clearly in Fig. 4, where the amount of hydrogen stored is plotted vs. the amount of surface oxygen groups. Then, the higher the oxygen amount in the samples, the lower the hydrogen uptake.

Taking into account the previous comments, and the fact that the surface oxygen complexes strongly affect the amount of hydrogen stored, we believe that not only the porosity is governing the process but also the surface chemistry of the material.

Table 2 shows the active surface area (ASA) for samples A, B and C6, which are the samples with different porosities and the initial lowest content in surface oxygen groups. It can be observed for these samples that the larger the active surface area, the higher the hydrogen uptake.

Therefore, all the results presented to the moment suggest that the actives sites of the material have an important role in the hydrogen trapping mechanism. Thus, if the active sites are saturated with surface oxygen groups, then they cannot contribute to the hydrogen storage. In this way, when a carbon material is thermally treated in inert atmosphere, the surface oxygen complexes are removed, generating unsaturated sites in the structure. These sites are especially reactive and can be used during the cathodic process in alkaline medium, where water molecules are reduced and the nascent hydrogen generated can interact with those reactive carbon atoms.

Thus, the active sites seem to control, at least partially, the hydrogen storage. It is known that porosity and active sites are related, since, as the porosity is developed, the amount of active sites increases. This could be the reason why acceptable correlations with either porosity or active sites are found. Moreover, when oxygen complexes are present in the sample,

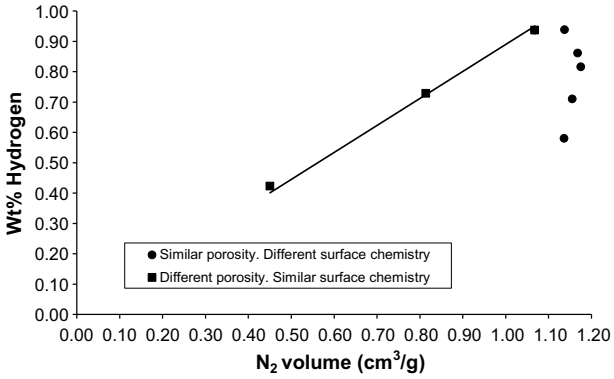

Fig. 3 – Weight% Hydrogen stored vs. V_{DR} N_2 volume.

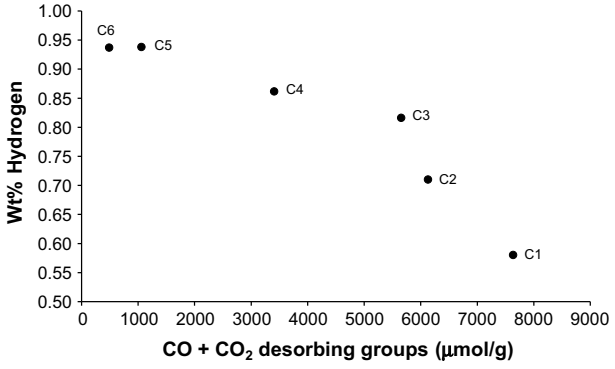

Fig. 4 – Weight% Hydrogen stored vs. CO + CO_2 desorbing groups.

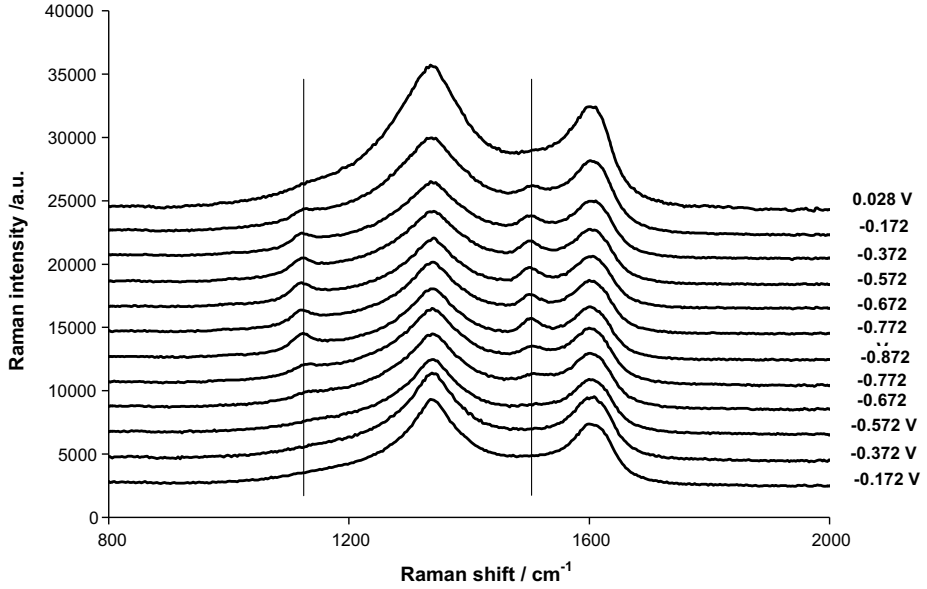

Fig. 5 – Raman spectra for sample C6 at different potentials. Excitation line = 632.8 nm, 6 M KOH.

the unsaturated sites become saturated and cannot be used for hydrogen chemisorption.

3.3. *In situ Raman spectroscopy characterization*

In order to confirm the above hypothesis, we have carried out in situ Raman spectroscopy experiments to follow the changes occurring on the carbon surface during the electrochemical charge and discharge processes. Fig. 5 plots the Raman spectra (632.8 nm) collected for sample C6 at different potentials, starting at −0.172 V. From this starting potential, it is changed to lower values into the reduction region to reach the water decomposition (hydrogen evolution) potential and, after that, the potential is changed to higher values until 0.028 V.

The Raman spectrum for the material at approximately −0.172 V, a potential very close to the open circuit one, shows the typical features for carbon materials [27]. Two broad and strongly overlapping bands at about 1350 cm^{-1} and at 1585 cm^{-1}, appear. These bands are associated to the graphitic D and G bands, respectively. The G band corresponds to an ideal graphitic lattice vibration mode, and the D band is known to be characteristic for disordered graphite.

Interestingly, as the potential decreases below −0.672 V, two bands appear simultaneously at about 1110 and 1500 cm^{-1}, which reach their maximum intensity at −0.872 V. This fact indicates that a structural change in the carbon material is taking place while the potential decreases. Similar bands have been observed in nano-diamond films formation and have been attributed to the C(sp^2)—H (υ1) bending vibration and the C=C (υ3) stretching vibration, respectively, in amorphous carbon—hydrogen bonds localized at grain boundary [28,29]. This suggests that the bands observed here are a consequence of the hydrogenation of carbon atoms forming C(sp^2)-H bonds. Interestingly, the potential at which the bands start to appear is very close to the potential at which

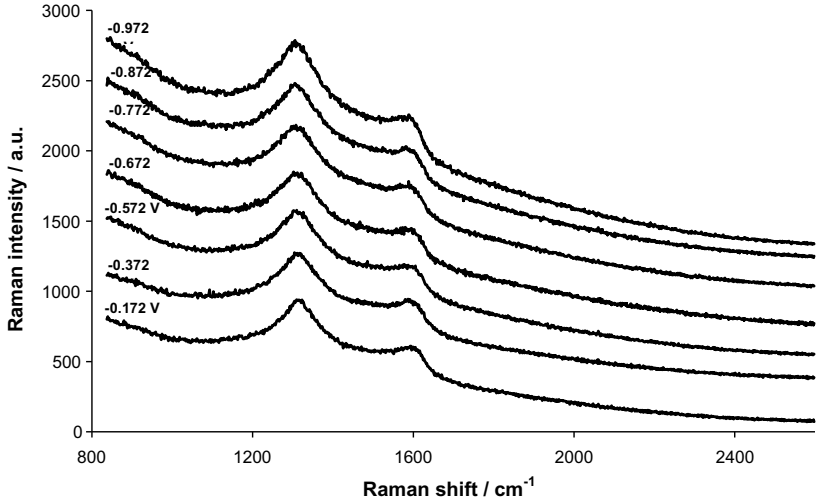

Fig. 6 – Raman spectra for sample C1 at different potentials. Excitation line = 784.8 nm, 6 M KOH.

Please cite this article in press as: Bleda-Martínez MJ et al., Effect of surface chemistry on electrochemical storage ..., Carbon (2008), doi:10.1016/j.carbon.2008.03.016

Faradaic formation of hydrogen from water is proposed (i.e., $H_2O + e^- \rightarrow H + OH^-$) [18].

Another interesting point observed with the Raman spectroscopy experiments is that the process is reversible and the bands disappear with increasing the potential (Fig. 5), as expected, taking into account the charge–discharge experiments.

Sample C1, the one with the highest content in surface oxygen groups, was also subjected to in situ Raman experiments. The results obtained are shown in Fig. 6. It can be observed that the bands corresponding to the C—H bonds are not observed in this case, at the experimental conditions used for the Raman measurements (i.e., shorter reaction time than in the charge–discharge experiments). However, from the amount of hydrogen stored in this sample (Table 2), these bands should be observed. The presence of oxygen complexes seems to impede the formation of the C—H bonds, being necessary longer reaction times and lower potentials to observe the C—H bands. Unfortunately, this cannot be done in the in situ Raman experiments performed since the accumulation of hydrogen bubbles impedes the surface observation. Additional work will be done in the future to modify the design of the in situ Raman cell to deepen into reaction mechanism.

4. Conclusions

The electrochemical hydrogen uptake of two series of porous carbon materials has been analysed. The first series of samples have similar surface chemistry and different porosity. The second one has similar porosities and different surface chemistry. Our results show that the electrochemical hydrogen storage is favoured in samples with a well developed porosity and a low content in surface oxygen complexes. Both features indicate that the unsaturated carbon atoms in the carbon materials have an important role for the hydrogen uptake.

In situ Raman spectroscopy allows us to conclude that C(sp^2)—H bonds are formed during the charge process. This chemisorption is reversible, and the original Raman spectrum of the carbon sample is recovered after the discharge step.

Acknowledgements

The authors thank MEC and FEDER for financial support (Project CTQ2006-08958/PPQ) and Ministerio de Fomento (70012/t05-fomento05 project). M.J.B.-M. thanks MEC for the thesis grant.

REFERENCES

[1] Miyake M. Electrochemical functions. In: Yosuda E, Inagaki M, Kaneko K, Endo M, Oya A, Tanabe Y, editors. Carbon Alloys. Amsterdam: Elsevier; 2003. p. 435–45.
[2] Frackowiak E, Beguin F. Carbon materials for the electrochemical storage of energy in capacitors. Carbon 2001;39:937–50.
[3] Conway BE. Electrochemical supercapacitors: scientific fundamentals and technological applications. New York: Kluwer Academic/Plenum Publishers; 1999.
[4] Bleda-Martínez MJ, Maciá-Agulló JA, Lozano-Castelló D, Morallón E, Cazorla-Amorós D, Linares-Solano A. Role of surface chemistry on electric double layer capacitance of carbon materials. Carbon 2005;43:2677–84.
[5] Chen X, Zhang Y, Gao XP, Pan GL, Jiang XY, Qu JQ, et al. Electrochemical hydrogen storage of carbon nanotubes and carbon nanofibers. Int J Hydrogen Energy 2004;29:743–8.
[6] Fazle Kibria AKM, Mo YH, Park KS, Nahm KS, Yun MH. Electrochemical hydrogen storage behaviors of CVD, AD and LA grown carbon nanotubes in KOH medium. Int J Hydrogen Energy 2001;26:823–9.
[7] Li S, Pan WY, Mao ZQ. A comparative study of the electrochemical hydrogen storage properties of activated carbon and well-aligned carbon nanotubes mixed with copper. Int J Hydrogen Energy 2005;30:643–8.
[8] Niessen RAH, de Jonge J, Notten P. The electrochemistry of carbon nanotubes I. Aqueous electrolyte. J Electrochem Soc 2006;153:A1484–91.
[9] Nutzenadel C, Zuttel A, Chartouni D, Schlapbach L. Electrochemical storage of hydrogen in nanotube materials. Electrochem Solid State Lett 1999;2:30–2.
[10] Youn HS, Ryu H, Cho TH, Choi WK. Purity enhancement and electrochemical hydrogen storage property of carbon nanofibers grown at low temperature. Int J Hydrogen Energy 2002;27:937–40.
[11] Zhang HY, Fu XJ, Yin JF, Zhou C, Chen YM, Li MH, et al. The effect of MWNTs with different diameters on the electrochemical hydrogen storage capability. Phys Lett 2005;339:370–7.
[12] Fang BZ, Zhou HS, Honma I. Ordered porous carbon with tailored pore size for electrochemical hydrogen storage application. J Phys Chem B 2006;110:4875–80.
[13] Jurewicz K, Frackowiak E, Beguin F. Enhancement of reversible hydrogen capacity into activated carbon through water electrolysis. Electrochem Solid State Lett 2001;4:A27–9.
[14] Frackowiak E, Beguin F. Electrochemical storage of energy in carbon nanotubes and nanostructured carbons. Carbon 2002;40:1775–87.
[15] Beguin F, Friebe M, Jurewicz K, Vix-Guterl C, Dentzer J, Frackowiak E. State of hydrogen electrochemically stored using nanoporous carbons as negative electrode materials in an aqueous medium. Carbon 2006;44:2392–8.
[16] Beguin F, Kierzek K, Friebe M, Jankowska A, Machnikowski J, Jurewicz K, et al. Effect of various porous nanotextures on the reversible electrochemical sorption of hydrogen in activated carbons. Electrochim Acta 2006;51:2161–7.
[17] Jurewicz K, Frackowiak E, Beguin F. Electrochemical storage of hydrogen in activated carbons. Fuel Process Technol 2002;77:415–21.
[18] Jurewicz K, Frackowiak E, Beguin F. Towards the mechanism of electrochemical hydrogen storage in nanostructured carbon materials. Appl Phys A – Mater Sci Process 2004;78:981–7.
[19] Vix-Guterl C, Frackowiak E, Jurewicz K, Friebe M, Parmentier J, Beguin F. Electrochemical energy storage in ordered porous carbon materials. Carbon 2005;43:1293–302.
[20] Miranda-Hernandez M, Rincon ME. Carbon paste electrodes: correlation between the electrochemical hydrogen storage capacity and the physicochemical properties of carbon blacks. J Solid State Electrochem 2005;9:646–52.
[21] Wu CZ, Zhu X, Ye LL, Ouyang CZ, Hu SQ, Lei LY, et al. Necklace-like hollow carbon nanospheres from the pentagon-including reactants: synthesis and electrochemical properties. Inorganic Chem 2006;45:8543–50.

[22] Lozano-Castello D, Lillo-Rodenas MA, Cazorla-Amoros D, Linares-Solano A. Preparation of activated carbons from Spanish anthracite I. Activation by KOH. Carbon 2001;39:741–9.
[23] Cazorla-Amoros D, Alcaniz-Monge J, de la Casa-Lillo MA, Linares-Solano A. CO_2 as an adsorptive to characterize carbon molecular sieves and activated carbons. Langmuir 1998;14:4589–96.
[24] Laine NR, Vastola FJ, Walker PL. Importance of active surface area in carbon–oxygen reaction. J Phys Chem B 1963;67:2030–4.
[25] Ehrburger P, Louys F, Lahaye J. The concept of active-sites applied to the study of carbon reactivity. Carbon 1989;27:389–93.
[26] Gomez R, Perez JM, Solla-Gullon J, Montiel V, Aldaz A. In situ surface enhanced Raman Spectroscopy on electrodes with platinum and palladium nanoparticle ensembles. J Phys Chem B 2004;108:9943–9.
[27] Sadezky A, Muckenhuber H, Grothe H, Niessner R, Poschl U. Raman micro spectroscopy of soot and related carbonaceous materials: Spectral analysis and structural information. Carbon 2005;43:1731–42.
[28] Kuzmany H, Pfeiffer R, Salk N, Gunther B. The mystery of the 1140 cm(−1) Raman line in nanocrystalline diamond films. Carbon 2004;42:911–7.
[29] Michaelson S, Hoffman A. Hydrogen bonding, content and thermal stability in nano-diamond films. Diamond Relat Mater 2006;15:486–97.

Please cite this article in press as: Bleda-Martínez MJ et al., Effect of surface chemistry on electrochemical storage ..., Carbon (2008), doi:10.1016/j.carbon.2008.03.016